PNAS
www.pnas.org

Main Manuscript for

Appraisal of sedimentary alkenones for the quantitative reconstruction of phytoplankton biomass

Maria Raja*[1] and Antoni Rosell-Melé[1,2]

[1] Institut de Ciència i Tecnologia Ambientals (ICTA-UAB), Universitat Autònoma de Barcelona, Bellaterra, Catalonia, Spain

[2] Institució Catalana de Recerca i Estudis Avançats (ICREA), Barcelona, Catalonia, Spain

* Maria Raja

Email: Maria.Raja@uab.cat

https://orcid.org/0000-0003-0207-8189

Classification

Physical Sciences, Environmental Sciences.

Keywords

primary productivity; proxy; remote sensing; global export and burial; marine sediments

Author Contributions

Maria Raja: Methodology, Software, Validation, Formal Analysis, Investigation, Data Curation, Writing-Original Draft, Writing-Review&Editing, Visualization.

Antoni Rosell-Melé: Conceptualization, Validation, Resources, Writing-Review&Editing, Supervision, Funding Acquisition.

This PDF file includes:

Main Text
Fig.s 1 to 5
Table 1

Abstract

Marine primary productivity is the driving factor in the global marine carbon cycle. Its reconstruction in past climates relies on biogeochemical proxies that are not considered to provide an unequivocal signal. These are often based on the water column flux of biogenic components to sediments (organic carbon, biogenic opal, biomarkers), although other factors than productivity are posited to control the sedimentary contents of the components, and their flux is related to the fraction of export production buried in sediments. Moreover, most flux proxies have not been globally appraised. Here we assess for the first time a proxy to quantify past phytoplankton biomass by correlating the concentration of C37 alkenones in a global suite of core-top sediments with sea-surface chlorophyll-*a* (SSchla) estimates over the last 20 years. SSchla is the central metric to calculate phytoplankton biomass and is directly related to primary productivity. We show that the global spatial distribution of sedimentary alkenones is primarily correlated to SSchla rather than diagenetic factors such as the oxygen concentration in bottom waters, which challenges previous assumptions on the role of preservation on driving concentrations of sedimentary organic compounds. Moreover, our results suggest that the rate of global carbon export to sediments is not regionally constrained, and that alkenones producers play a dominant role in the global export of carbon buried in the sea-floor. This study shows the potential of using sedimentary alkenones to estimate past phytoplankton biomass, which in turn can be used to infer past primary productivity (PP) in the global ocean.

Significance Statement

Biomarker proxies, namely alkenones, are commonly used to reconstruct past primary productivity. However, their value has been questioned as they are posited to be controlled by diagenetic processes and often limited to draw qualitative inferences on the carbon cycle. In fact, most proxies have not been globally appraised with ocean biogeochemical data. Here we use a combination of remote sensing and geochemical data to provide the first spatial-based global calibration that show the use of alkenones to quantify past sea-surface chlorophyll-*a* concentration, which ultimately can be used to infer quantitatively past primary productivity in paleorecords. This calibration paves the way to clarify the relative role of the marine carbon cycle in climate variability using field data, and test biogeochemical models.

Main Text

Introduction

Global carbon distribution between the ocean and the atmosphere regulates global climate on Earth. This distribution is primarily controlled by marine primary productivity (PP) and phytoplanktonic organisms, which transforms atmospheric CO_2 into organic matter. Only a fraction of this produced organic matter is exported to the deep ocean. Global models estimate that 48 $PgC \cdot yr^{-1}$ are produced in ocean surface waters (1) while 6 $PgC \cdot yr^{-1}$ (2) are exported out from the photic zone, and 0.15 $PgC \cdot yr^{-1}$ are buried in sediments (3). Exported organic carbon is out of contact with the atmosphere on decadal to millennial timescales or longer once is buried in

the seafloor, which exerts a major control on global climate by regulating the partial pressure of atmospheric CO_2 (4). Hence, estimating marine PP, export and burial productivity changes during past key climatic periods (e.g. glacial-interglacial transitions) is essential to understand our present climate and predict its evolution in the future.

To infer past PP a range of proxies based on the fluxes of biogenic components are available (5–7). As flux proxies, they are related to changes in past export productivity, which are assumed to be proportional to surface PP in paleoreconstructions. However, depositional factors such as oxygen or ballasting effect are thought to be important in controlling organic matter export from the upper water column to sediments (8–10) and thus, organic proxies sedimentary concentration. The relative weights that control the spatial variability of organic matter concentration in sediments, are still unconstrained, which leads to some uncertainty on the applicability of organic matter proxies to infer PP (7). Consequently, available proxies are sometimes interpreted to infer either changes in PP or depositional conditions (11).

One of the common approaches to reconstruct PP relies on the measurement of C_{37} di- and tri-unsaturated methyl ketones (i.e. C_{37} alkenones) concentrations or fluxes in sediments (12–18). These organic molecules are biomarkers of the ubiquitous coccolithophore *Emiliania huxleyi*, which is the principal source of alkenones and the most abundant coccolithophore in the modern pelagic ocean (19–24). *Geophyrocapsa oceanica* and other coccolithophoral species from the same genera are also considered important alkenones producers nowadays (20).

In this study, we evaluate for the first time the potential use of sedimentary C_{37} alkenones contents to infer past phytoplankton biomass at a global scale through the comparison of their spatial variability in a global compilation of core-top sediments with sea-surface chlorophyll-*a* (SSchla) (Fig. 1). This is the primary pigment of photosynthesis and is present in all photosynthetic phytoplankton species. Its concentration in surface waters is commonly used as an indicator of phytoplankton biomass and to infer primary productivity (25, 26). On a global scale, its concentration in surface waters is estimated by remote sensing (27). We also assess the effect of oxygen on the spatial accumulation of alkenones in sediments by comparing its concentration in bottom waters with alkenones abundance on a global scale.

Results

Global comparison of SSchla with sedimentary alkenones

The comparison between sedimentary alkenones and SSchla concentration estimated over the last 20 years is shown in Fig. 2. Log-transformation was needed, as the distribution of SSchla is close to lognormal in our dataset (SI Appendix, Fig. S1). This is concordant with the natural distribution of ocean chlorophyll (28). We applied standard major axis regressions (Type II regressions), which assume that both variables are measured and include some error. For this analysis we took into account that the remote sensing SSchla estimates using global standard algorithms can have a wide range of error values and specific regional biases (29–35). To minimize uncertainty in the correlation analysis, we focused our study on SSchla data located in well-performing remote sensing regions. We applied the threshold stablished in (36), where basins associated with lower
root-mean square logarithmic errors (RMS log errors) than the global mean (31%), are considered well-performing regions. This value is within the range of 30-35% threshold values proposed in the remote sensing literature, including the Global Climate Observing System (GCOS) and the Ocean Colour Climate Change Initiative (OC-CCI), as the desired error benchmark for open ocean waters, or optically clear waters (30, 31, 36–38). Consequently, we did not included in our final analysis (see Fig. 2b) SSchla data from the North Atlantic (36, 39, 40) and the Gulf of Alaska (41).Nor from the western South American margin, as the SSchla error estimate of this region has not been thoroughly studied. Although data for the equatorial Atlantic presents a RMS log error of 48%, it lowers to 23% when removing samples located offshore of the north-eastern coast of South America (36). Thus, as our samples are not located in this region, we included samples from the equatorial Atlantic in the correlation analysis. We obtained

a linear correlation between C_{37} alkenones and SSchla concentration with an RMS log error of 38% and a coefficient of determination (R^2) of 0.60 (Table 1). Hence, our data show that changes in the spatial variability of C_{37} alkenones are mainly related to changes in SSchla.

Several studies report the occurrence of regional variability in the vertical attenuation rate of organic matter flux from the surface to the deep ocean (10, 42–44). This spatial variability could lead to different regional correlations between sedimentary alkenones and SSchla concentration. To investigate this issue in our data set, we divided the data by biogeochemical regions as defined in (44), which are classified by factors influencing transfer efficiency, such as phytoplankton community, nutrient concentration and temperature. The defined regions are as follows: the tropics, the subtropics, the subarctic and the Southern Ocean. Note that the correlation for the subarctic region was not calculated due to insufficient data. The data from the subtropics show the lower RMS log error (31%) and is the region that can explain more SSchla variability (59%). The tropics present the higher RMS log error (46%), with a coefficient of determination of 0.49, and the Southern Ocean is the region that can explain less SSchla variability (33%), with a log RMS error of 35% (Table 1). However, no significant differences were found between sedimentary alkenones and SSchla correlations when comparing different oceanic biogeochemical regions, as it is shown in Fig. 3.

Global comparison of bottom water oxygen with sedimentary alkenones

To study the influence of oxygen in the spatial accumulation of alkenones in sediment, we correlated our global core-top sedimentary alkenones compilation with oxygen concentration in bottom waters (Fig. 4). Data on oxygen concentration was extracted from the World Ocean Atlas 2018, which provide oxygen data with a spatial resolution of 1º. The relative low resolution of the data may introduce some uncertainty in our analyses in some regions, as strong oxygen gradients may occur that are smaller than the 1º grid of the dataset, such as those located in oceanic ridges. However, our data do provide information about the influence of bottom oxygen content on alkenones abundance at regional and global scales.

The global comparison between sedimentary alkenones and oxygen concentration in bottom waters is shown in Fig. 4. Since our study comprises several biogeochemical regions (Fig. 1), it covers a wide range of oxygen concentration conditions (from 18.72 to 268.11 $\mu mol \cdot kg^{-1}$). Consequently, Fig. 4 shows different patterns that might reflect the influence of oxygen concentration in different regions. Nevertheless, we do not observe a simple global overall trend as in the case of SSchla, and we obtained a R^2 of 0.02. Thus, oxygen concentration in bottom waters is not the primary cause of alkenones abundance spatial variability on a global scale.

Discussion

Alkenones as a proxy for past phytoplankton biomass

Alkenones concentration in sediments is commonly used to qualitatively infer PP changes (14, 17, 18). However, as it is commonly stated in the literature, sedimentary alkenones concentration may also be affected by depositional and burial processes, which could complicate the interpretation of the proxy. Thus, alkenones concentration fluxes decrease with depth in the water column (45, 46). In here, we do not appraise directly the link between PP and alkenones sedimentary concentration, but indirectly through the use of SSchla which is a metric of phytoplankton biomass (Fig. 2). The data span several oceanic biogeochemical regions (44), and show that the spatial variability in sedimentary alkenones is primarily related to changes in SSchla, following a linear relationship with a R^2 of 0.60 and RMS log error of 38% (Table 2). Our data permit to quantitatively reconstruct past SSchla concentration (equation 2). Therefore, our results confirm previous assumptions on the use of sedimentary alkenones concentrations as a proxy to qualitatively infer PP changes rather than redox conditions.

The correlations in Fig. 2 also allow the quantitative comparison of phytoplankton biomass data from different sites and regions through time, which hitherto was considered hindered by differences in depositional conditions between locations. Thus, one of the implications of

obtaining a global correlation between C_{37} alkenones and SSchla concentrations is that the vertical rate of degradation of C_{37} alkenones from the sea-surface to sediments follows a similar spatial pattern across different biogeochemical regions in the global ocean. We have obtained no significantly different correlations between C_{37} alkenones and SSchla concentration for the different oceanic biogeochemical regions defined in (44) (Fig. 3). This is consistent with studies that have indicated that there are no regional differences in the vertical attenuation rate of organic matter flux (47–49), even though other studies have found spatial variability in the export efficiency of surface biomass to the deep ocean (10, 42–44).

Hence, our data support the results obtained in (50) and other earlier papers, which showed that spatial variability in the vertical flux of particulate organic carbon decreases with increasing water column depth. Our results are also in agreement with (51), who showed that the proportion of primary productivity that reaches the deep sea does not vary greatly with latitude in the North Atlantic. Besides, these results show that the global correlation is independent of the biogeographic region, which implies that it is applicable globally despite any changes in biogeochemical regions through time. In this sense, we assume the similar pattern of the vertical degradation rate over different biogeochemical regions is also maintained after burial processes. Future studies will evaluate to which extent subsurface degradation process might significantly influence or bias the relationships described in Fig.s 2 and 3, and constrain their application in paleo studies.

The relevant role of alkenones producers in the global carbon export

In contrast to SSchla, alkenones are mainly produced by coccolithophores (*E. huxleyi* and *Geophyrocapsa species*) (20). Therefore, sedimentary alkenones concentration are often considered an exclusive coccolithophore productivity proxy, which may not provide information about total past phytoplanktonic biomass changes (15, 18, 52, 53). In contrast, C_{37} alkenones concentration were also suggested to track PP not only from coccolithophores, but also from the wider phytoplanktonic community in upwelling tropical areas (12). Subsequently, such interpretation was corroborated at two more sites: ODP Site 982 in the North Atlantic and ODP Site 846 in the eastern tropical Pacific (54). In spite of their findings, the authors suggested a linear relationship would be not expected in oligotrophic areas, where alkenone-synthesising coccolithophores constitute a small proportion of the coccolithophore population.

Contrary to previous assumptions, our global correlation shows that C_{37} alkenones sedimentary concentrations can be interpreted as a proxy for total phytoplankton biomass in different biogeochemical regions (Fig. 2), and suggests that there are no differences between samples located in oligotrophic (SSchla annual average < 0.1 $mg \cdot m^{-3}$) and non-oligotrophic regimes (SI Appendix, Fig. S2).

Obtaining a global correlation between SSchla and alkenones indicates a proportionality between total phytoplankton biomass and alkenones accumulation in sediments. In terms of total phytoplankton biomass and PP, photosynthetic picoeukaryotes, which include *E. huxleyi* and *G. oceanica*, have been reported to be the dominant contributors. For instance, photosynthetic picoeukaryotes are responsible for more than the half the total PP in the North Atlantic (68%) (55), southern California Bight (76%) (56), the eastern northatlantic subtropical gyre (54%) (57), the southern Bay of Biscay (51%) (58) and the South East Pacific Ocean (>60%) (59).

However, there is not a consensus on which class of phytoplankton is the dominant carbon exporter to the sea floor. Large phytoplankton, such as diatoms, were recognised to dominate global carbon export to sediments (60, 61) and picoplankton (photosynthetic picoeukaryotes and cyanobacteria) were claimed not to contribute significantly to carbon export because of their small size (62). In contrast, more recent studies have suggested that picoplankton plays a major role in the sedimentary carbon fluxes. For instance, massive picoplankton sedimentation in east of New Zealand (63), and picoplankton export carbon fluxes dominance were found in the eastern equatorial Pacific (64) and in the Arabian sea (65). Besides, subsequent studies showed that the downward flux of organic carbon via small particles often constitutes the bulk of the total

particulate organic carbon flux in the North Atlantic (66), and that the export of small particles in the Norwegian Sea contributed to long-term carbon sequestration (67).

We are not aware of any evidence that endorse the notion that alkenones producers are one of the main contributors to global carbon sequestration. However, our results in Fig. 2 indicate that alkenones producers export and burial contribution is proportional to total phytoplankton biomass at global scale. Our results are in agreement to previous findings that show primary productivity to be proportional to picoplankton biomass export from the euphotic zone at two different locations: the equatorial Pacific and the Arabian Sea (68). We suggest that such proportionality is indicative of the putative dominant role of photosynthetic picoeukaryotes to global carbon sequestration and burial in the sea-floor.

The role of oxygen in the spatial accumulation of alkenones in sediment

Oxygen enhances organic matter degradation and its concentration in bottom waters is considered a key factor in the preservation and accumulation of organic matter in sediments (69–73). However, despite its strong influence in the vertical degradation of organic matter, its role in the global spatial distribution of organic matter concentration remains unconstrained.

Some studies located in oxygen minimum zones, such as the Arabian Sea, reported empirical relationships between oxygen concentration in bottom waters and sedimentary organic matter or alkenones concentration (69, 74–76). Although these relationships only show a correlation when oxygen is present at very low concentrations (≤ 50 $\mu mol \cdot kg^{-1}$), alkenones concentration is sometimes used to reconstruct preservation conditions in other environments, such as the Pacific and the Atlantic oceans (11, 77, 78).

Our results in Fig. 4 show that there is not a straightforward relationship between the spatial concentration patterns of sedimentary alkenones and bottom water oxygen. In contrast to previous studies, our data are located in different oceanic biogeochemical regions and include low and high oxygen content environments (from 19 to 268 $\mu mol \cdot kg^{-1}$). Therefore, the wide range of oxygen concentration presented in this study would be much more representative of the global ocean conditions than those previously evaluated. These results can be interpreted as evidence of the minor role of oxygen concentration in the spatial distribution of sedimentary alkenones for the greater part of the ocean. Thus, our data do not support the global use of alkenones concentration to reconstruct preservation conditions in the deep ocean.

Conclusions

The primary driver explaining the global spatial distribution of sedimentary alkenones is phytoplankton biomass as reflected by SSchla concentration. Different biogeographic regions do not show significant differences in their correlations between sedimentary alkenones and SSchla concentration. Moreover, oxygen concentration in bottom waters does not strongly influence the spatial concentration of alkenones in sediments on a global scale. Hence, our results do support the use of alkenones sedimentary abundance to study primary productivity, and do not support the use of alkenones as an indicator of preservation conditions in the deep ocean. Besides, our data indicate that the global vertical attenuation rate of organic matter flux from sea-surface to sediments is not regionally constrained, and suggest that the global carbon export and burial is dominated by photosynthetic picoeukaryotes.

Thus, this study provides the first spatial-based global calibration that show the use of sedimentary alkenones to quantify sea-surface chlorophyll-*a*, which ultimately can be used to infer quantitatively PP in paleorecords. This calibration is independent of biogeographic regions, which implies that besides relative PP changes through downcore, it can also be used for the spatial comparison of PP between different locations at any site in the global ocean. Furthermore, it is applicable despite any putative changes in biogeochemical regions through time.

Materials and Methods

Sedimentary alkenones

We compiled alkenone data from 226 locations widely distributed around the global ocean, and across diverse biogeochemical regions as defined in (44) (Fig. 1). Most of the data are obtained from previous published studies (95% of the compilation), while the rest were analysed in our laboratory following the methodology explained hereafter. We assume that the interlaboratory reproducibility of the different available methods to measure the absolute alkenones abundance in sediments is 32% (79). The samples in the compilation generally correspond to the upper 1 cm of a sediment core, and approximately 90% of them were retrieved using devices specially designed for a minimum disturbance of the sediment surface, i.e. box corer or multicorer. The compilation appears to be dominated by samples along continental margins, since they represent the most intensively studied regions. However, sample sites span a wide range of alkenones concentration distributed in the diverse biogeochemical regions defined in Weber et al. (2016) around the global ocean (Fig. 1). In addition, over 80% of the compiled surface sediments are in sites with a water column deeper than 1,000 meters, while over 90% of the samples were retrieved from waters deeper than 500 meters (SI Appendix, Dataset S1). Consequently, the compilation is mainly representative of the water column of the open ocean. We estimate that in average, a sedimentary sample represents a time span of sedimentation of ca. 71 years. This has been obtained from the sedimentation rate average of all sediments (14 $cm \cdot ka^{-1}$) using the map published in (80). However, variability of sedimentation rates could play a role in driving the concentration of alkenones in sediments. Consequently, to analyse changes in the flux of a chemical or substance to the sea, the mass accumulation rates (MAR) must be used instead of concentrations. Alkenones mass accumulation rates (MARalkenones) were estimated by multiplying alkenones concentration by sedimentation rate and dry bulk density. In the absence of these data for each sample site, we extracted sedimentation rates from two global maps previously published (51, 80) and discussed in (81). However, sedimentation rates could only be extracted for 54% of the sites. Dry bulk densities were assumed to be 0.9 $g \cdot cm^{-3}$, as it corresponds to the mean dry bulk density for marine sediments in the global sediment core database published in (81), which has been created by retrieving available data from online data repositories. It is important to point out that these estimated accumulation rates are highly uncertain, given that sedimentation rates can vary significantly over relatively short distances on the seafloor due to winnowing and focusing, and the locations of cores are often biased towards the highest accumulation rates in the search of retrieving records with high temporal resolution. Nonetheless, in the absence of more accurate data, we include the estimates to provide a first-order information on the effect of sedimentation rates in our compilation. We compared MARalkenones against alkenones concentration in SI Appendix, Fig. S3. The correlation between the two variables is high as attested by their coefficient of determination of R^2=0.92 and R^2=0.87, depending on the sources of sedimentation rates (51, 80). Consequently, overall for our compilation, the differences in using MARalkenones and alkenones concentration when compared to values of SSchla concentration are not likely to lead to significantly different results. To maximize the size of data points in our compilation we used the alkenones concentration rather than its MAR.

In the samples analysed for the study, sediments (1-4 g) were extracted using 10 mL of a mixture of dichloromethane and methanol (3:1) (GC grade, Suprasolv) in a MARS5 microwave accelerated extraction system (CEM Corporation). Before extraction, 25 $ng \cdot \mu L^{-1}$ of the internal standard 2-nonadecanone (Fluka, purity 0.97%) was added to the sediment placed in a Teflon vessel. During extraction the mixture was stirred continuously with a magnetic bar, while temperature was increased from ambient to 70ºC for 2.5 minutes and left at this temperature for a further 5 minutes. After extraction, samples' vessels were left to cool down at room temperature, and the supernatants were decanted into glass tubes and centrifuged. Extracts were then dried under vacuum and cleaned up using SiO_2 columns eluted sequentially with hexane (first fraction) and dichloromethane (second fraction). Extracts were dried again and 50 µL of isooctane was added to the second fraction before their analysis with a gas chromatograph (GC) fitted with a

flame ionization detector at 320ºC (Agilent Technologies 7820A GC System). Samples were injected in splitless mode in a GC column (HP-1 GC column, 60m length, 250µm internal diameter, 0.25µm film thickness) with a flow rate of 1.5 $mL \cdot min^{-1}$. The GC method consists of 2 ramps, the first one from 80ºC to 120ºC with a temperature rate of 30 $ºC \cdot min^{-1}$, followed by a second ramp that increases temperature at 6ºC min^{-1} until 320ºC, and held at this temperature during 21 minutes.

Ocean surface chlorophyll

Satellite observation of ocean-colour, in the open ocean, is primarily dependent on phytoplankton occurrence. These unicellular algae contain photosynthetic pigments, primarily chlorophyll-*a*, which coexist together with other pigments, associated detrital, and coloured dissolved organic matter (82). To infer SSchla from ocean-colour data, many algorithms have been constructed relating characteristics of the water signal to the property of interest (83). There are large uncertainties in the estimation of SSchla in some regions, particularly where the optical and biological properties are complex (84, 85). For instance, some of the factors that affect the properties of the surface waters are coloured dissolved organic matter, radiance-absorbing aerosols, phytoplankton species diversity, suspended sediments and minerals, clouds, ice, sun glint, and navigation/time space mismatches (86–89). Furthermore, desert dust (90) and bubbles (91) make the water appear greener. Other sources of scatter are the remote sensing limitation of detecting SSchla at different depths in the water column (92, 93).

Global SSchla algorithms, calibrated with global *in situ* datasets, show average root mean square (RMS) log errors of 34% (29). The Global Climate Observing System uncertainty requirement for SSchla is 30% (www.ncdc.noaa.gov/gosic/gcos-essential-climate-variable-ecv-data-access-matrix/gcos-ocean-biogeochemistry-ecv-ocean-color). End-users of SSchla data commonly *quote* uncertainty requirement of 35% (83). There are a number of challenges in the calibration of remote sensing data, like the diversity of optical properties in various water types, comparability of ocean *in situ* measurements using different analytical approaches, and the different spatial and temporal scales of the ocean-in situ and satellite measurements (83).

The available ocean colour satellite data since 1997 have been merged in the GlobColour project (http://globcolour.info), which combines measurements from the Sea-viewing Wide Field-of-view Sensor (SeaWiFS; 1997-2010), the MEdium Resolution Imaging Spectrometer (MERIS; 2002-2012), the MODerate-resolution Imaging Spectroradiometer (MODIS; 2002-2017), and the Visible Infrared Imaging Radiometer Suite (VIIRS; 2012-2017) missions. The spatial resolution of the available data for end-users is 1/24º (4.63 km at the equator). The algorithms used for obtaining SSchla are OC4v5 for SeaWiFS, OC4Me for MERIS and OC3v5 for MODIS and VIIRS (94). SSchla values for every sediment location were extracted from merged global-scale matrixes of the Globcolour Project, which contain monthly data. For this paper, we extracted SSchla concentration data from September 1997 to December 2017 for every core location. GlobColour data used in this study have been developed, validated, and distributed by ACRI-ST, France. We used the Matlab script provided by the Monterey Bary Aquarium Research Institute (https://www.mbari.org/index-of-downloadable-files/) to calculate the standard major axis regressions (type II regressions) between SSchla and sedimentary alkenones.

Acknowledgments

This research used samples provided by the OSU-MGR Collection and the Scripps Institution of Oceanography and the Integrated Ocean Drilling Program (IODP). We are in debt with Niko Lahajnar and Zanna Chase for providing samples. We also thank Eric D. Galbraith and Markus Kienast for their insightful comments and discussion. GlobColour data (http://globcolour.info) used in this study have been developed, validated, and distributed by ACRI-ST, France. Ocean Data View is acknowledged for providing software. We acknowledge financial support from the

European Research Council (PALADYN-834934), the Spanish research Ministry (CTM2013-43006-P) and the Spanish Ministry of Science, Innovation and Universities, through the “María de Maeztu” program for Units of Excellence (MDM-2015-0552).

The authors declare no competing interest.

References

1. J. L. Sarmiento, N. Gruber, *Ocean Biogeochemical Dynamics* (Princeton Univ. Press, 2006) https:/doi.org/10.1063/1.2754608.
2. D. A. Siegel, *et al.*, Global assessment of ocean carbon export by combining satellite observations and food-web models. *Global Biogeochem. Cycles* **28**, 181–196 (2014).
3. F. E. Muller-Karger, *et al.*, The importance of continental margins in the global carbon cycle. *Geophys. Res. Lett.* **32**, 1–4 (2005).
4. P. W. Boyd, H. Claustre, M. Levy, D. A. Siegel, T. Weber, Multi-faceted particle pumps drive carbon sequestration in the ocean. *Nature* **568**, 327–335 (2019).
5. K. E. Kohfeld, C. Le Quéré, S. P. Harrison, R. F. Anderson, Role of marine biology in glacial-interglacial CO2cycles. *Science (80-.).* **308**, 74–78 (2005).
6. M. Zhao, J. L. Mercer, G. Eglinton, M. J. Higginson, C. Y. Huang, Comparative molecular biomarker assessment of phytoplankton paleoproductivity for the last 160 kyr off Cap Blanc, NW Africa. *Org. Geochem.* **37**, 72–97 (2006).
7. S. D. Schoepfer, *et al.*, Total organic carbon, organic phosphorus, and biogenic barium fluxes as proxies for paleomarine productivity. *Earth-Science Rev.* **149**, 23–52 (2015).
8. T. DeVries, T. Weber, The export and fate of organic matter in the ocean: New constraints from combining satellite and oceanographic tracer observations. *Global Biogeochem. Cycles* **31**, 535–555 (2017).
9. R. Francois, S. Honjo, R. Krishfield, S. Manganini, Factors controlling the flux of organic carbon to the bathypelagic zone of the ocean. *Glob. Biogeochem. Cycles* **16**, 1087 (2002).
10. S. A. Henson, R. Sanders, E. Madsen, Global patterns in efficiency of particulate organic carbon export and transfer to the deep ocean. *Global Biogeochem. Cycles* **26**, 1–14 (2012).
11. R. F. Anderson, *et al.*, Deep-Sea Oxygen Depletion and Ocean Carbon Sequestration During the Last Ice Age. *Global Biogeochem. Cycles* **33**, 301–317 (2019).
12. C. T. Bolton, *et al.*, Glacial-interglacial productivity changes recorded by alkenones and microfossils in late Pliocene eastern equatorial Pacific and Atlantic upwelling zones. *Earth Planet. Sci. Lett.* **295**, 401–411 (2010).
13. K. T. Lawrence, Evolution of the Eastern Tropical Pacific Through Plio-Pleistocene Glaciation. *Science (80-.).* **312**, 79–83 (2006).
14. A. Moreno, I. Cacho, M. Canals, J. O. Grimalt, A. Sanchez-Vidal, Millennial-scale variability in the productivity signal from the Alboran Sea record, Western Mediterranean Sea. *Palaeogeogr. Palaeoclimatol. Palaeoecol.* **211**, 205–219 (2004).
15. B. Petrick, *et al.*, Oceanographic and climatic evolution of the southeastern subtropical Atlantic over the last 3.5 Ma. *Earth Planet. Sci. Lett.* **492**, 12–21 (2018).
16. F. G. Prahl, R. B. Collier, J. Dymond, M. Lyle, M. A. Sparrow, A biomarker perspective on prymnesiophyte productivity in the northeast pacific ocean. *Deep. Res. Part I* **40**, 2061–2076 (1993).
17. F. Rostek, E. Bard, L. Beaufort, C. Sonzogni, G. Ganssen, Sea surface temperature and productivity records for the past 240kyr in the Arabian Sea. *Deep. Res.* **44**, 1461–1480 (1997).
18. O. Seki, *et al.*, Reconstruction of paleoproductivity in the Sea of Okhotsk over the last 30 kyr. *Paleoceanography* **19** (2004).

19. S. Schmidt, *et al.*, Particle export during a bloom of Emiliania huxleyi in the North-West European continental margin. *J. Mar. Syst.* **109**–**110**, S182–S190 (2013).
20. J. K. Volkman, S. M. Barrett, S. I. Blackburn, E. L. Sikes, Alkenones in Gephyrocapsa-Oceanica - Implications for Studies of Paleoclimate. *Geochim. Cosmochim. Acta* **59**, 513–520 (1995).
21. J. K. Volkman, G. Eglinton, E. D. S. Corner, T. E. V. Forsberg, Long-chain alkenes and alkenones in the marine coccolithophorid Emiliania huxleyi. *Phytochemistry* **19**, 2619–2622 (1980).
22. I. T. Marlowe, *et al.*, Long chain (n-c37-c39) alkenones in the prymnesiophyceae. distribution of alkenones and other lipids and their taxonomic significance. *Br. Phycol. J.* **19**, 203–216 (1984).
23. L. L. Rhodes, B. M. Peake, A. L. MacKenzie, M. Simon, A. R. Edwards, Coccolithophores Gephyrocapsa oceanica and Emiliania huxleyi (Prymnesiophyceae = Haptophyceae) in New Zealand's coastal waters: Characteristics of blooms and growth in laboratory culture. *New Zeal. J. Mar. Freshw. Res.* **29**, 345–357 (1995).
24. M. H. Conte, J. K. Volkman, G. Eglinton, Lipid biomarkers of the Prymnesiophyceae. *The Haptophyte Algae* **51**, 351–377 (1994).
25. M. J. Behrenfeld, E. Boss, D. A. Siegel, D. M. Shea, Carbon-based ocean productivity and phytoplankton physiology from space. *Global Biogeochem. Cycles* **19**, 1–14 (2005).
26. Y. Huot, *et al.*, Relationship between photosynthetic parameters and different proxies of phytoplankton biomass in the subtropical ocean. *Biogeosciences* **4**, 853–868 (2007).
27. Z. Lee, J. Marra, M. J. Perry, M. Kahru, Estimating oceanic primary productivity from ocean color remote sensing: A strategic assessment. *J. Mar. Syst.* **149**, 50–59 (2015).
28. J. W. Campbell, The lognormal distribution as a model for bio-optical variability in the sea. *J. Geophys. Res.* **100**, 13237–13254 (1995).
29. R. J. W. Brewin, *et al.*, Uncertainty in Ocean-Color Estimates of Chlorophyll for Phytoplankton Groups. *Front. Mar. Sci.* **4** (2017).
30. S. Dutkiewicz, A. E. Hickman, O. Jahn, Modelling ocean-colour-derived chlorophyll a. *Biogeosciences* **15**, 613–630 (2018).
31. Global Climate Observing System, "Systematic Observation Requirements For Satellite-Based Data Products for Climate - 2011 Update" (2011).
32. IOCCG, *Partition of the Ocean into Ecological Provinces : Role of Ocean-Colour Radiometry*, M. Dowell, T. Platt, Eds. (Reports ofthe International Ocean-Colour Coordinating Group, No. 9, IOCCG, 2009).
33. T. Jackson, S. Sathyendranath, F. Mélin, "An improved optical classification scheme for the Ocean Colour Essential Climate Variable and its applications" (Elsevier Inc., 2017).
34. T. Moore, J. Campbell, M. Dowell, A class-based approach to characterizing and mapping the uncertainty of the MODIS ocean chlorophyll product. *Remote Sens. Environ.* **113**, 2424–2430 (2009).
35. I. Shulman, *et al.*, Bio-Optical Data Assimilation With Observational Error Covariance Derived From an Ensemble of Satellite Images. *J. Geophys. Res. Ocean.* **123**, 1801–1813 (2018).
36. W. W. Gregg, N. W. Casey, Global and regional evaluation of the SeaWiFS chlorophyll data set. *Remote Sens. Environ.* **93**, 463–479 (2004).
37. C. Hu, L. Feng, Z. Lee, Uncertainties of SeaWiFS and MODIS remote sensing reflectance: Implications from clear water measurements. *Remote Sens. Environ.* **133**, 168–182 (2013).
38. C. R. McClain, A Decade of Satellite Ocean Color Observations. *Ann. Rev. Mar. Sci.* **1**, 19–42 (2009).
39. M. Stramska, D. Stramski, H. Ryszard, S. Kaczmarek, S. Joanna, Bio-optical relationships and ocean color algorithms for the north polar region of the Atlantic. *J. Geophys. Res.* **108**, 3143 (2003).
40. A. Mendonça, *et al.*, Evaluation of ocean color and sea surface temperature sensors algorithms using in situ data: a case study of temporal and spatial variability on two

northeast Atlantic seamounts. *J. Appl. Remote Sens.* **4**, 043506 (2010).
41. J. N. Waite, F. J. Mueter, Spatial and temporal variability of chlorophyll-a concentrations in the coastal Gulf of Alaska, 1998-2011, using cloud-free reconstructions of SeaWiFS and MODIS-Aqua data. *Prog. Oceanogr.* **116**, 179–192 (2013).
42. P. J. Lam, S. C. Doney, J. K. B. Bishop, The dynamic ocean biological pump: Insights from a global compilation of particulate organic carbon, CaCO3, and opal concentration profiles from the mesopelagic. *Global Biogeochem. Cycles* **25**, 1–14 (2011).
43. C. M. Marsay, *et al.*, Attenuation of sinking particulate organic carbon flux through the mesopelagic ocean. *Proc. Natl. Acad. Sci.* **112**, 1089–1094 (2015).
44. T. Weber, J. A. Cram, S. W. Leung, T. DeVries, C. Deutsch, Deep ocean nutrients imply large latitudinal variation in particle transfer efficiency. *Proc. Natl. Acad. Sci.* **113**, 8606–8611 (2016).
45. M. Yamamoto, *et al.*, Seasonal and depth variations in molecular and isotopic alkenone composition of sinking particles from the western North Pacific. *Deep. Res. Part I Oceanogr. Res. Pap.* **54**, 1571–1592 (2007).
46. P. J. Müller, G. Fischer, A 4-year sediment trap record of alkenones from the filamentous upwelling region off Cape Blanc, NW Africa and a comparison with distributions in underlying sediments. *Deep. Res. Part I Oceanogr. Res. Pap.* **48**, 1877–1903 (2001).
47. E. Suess, Particulate organic carbon flux in the oceans—surface productivity and oxygen utilization. *Nature* **288**, 260–263 (1980).
48. J. H. Martin, G. A. Knauer, D. M. Karl, W. W. Broenkow, VERTEX: carbon cycling in the northast Pacific. **34**, 267–285 (1987).
49. R. S. Lampitt, A. N. Antia, Particle flux in deep seas: Regional characteristics and temporal variability. *Deep. Res. Part I Oceanogr. Res. Pap.* **44**, 1377–1403 (1997).
50. M. Lutz, R. Dunbar, K. Caldeira, Regional variability in the vertical flux of particulate organic carbon in the ocean interior. *Global Biogeochem. Cycles* **16**, 11-1-11–18 (2002).
51. R. A. Jahnke, The global ocean flux of particulate organic carbon : Areal distribution and magnitude. **10**, 71–88 (1996).
52. C. Pelejero, J. O. Grimalt, M. Sarnthein, L. Wang, J. A. Flores, Molecular biomarker record of sea surface temperature and climatic change in the South China Sea during the last 140,000 years. *Mar. Geol.* **156**, 109–121 (1999).
53. M. J. Higginson, M. A. Altabet, Initial test of the silicic acid leakage hypothesis using sedimentary biomarkers. *Geophys. Res. Lett.* **31**, 4–7 (2004).
54. C. T. Bolton, K. T. Lawrence, S. J. Gibbs, P. A. Wilson, T. D. Herbert, Biotic and geochemical evidence for a global latitudinal shift in ocean biogeochemistry and export productivity during the late Pliocene. *Earth Planet. Sci. Lett.* **308**, 200–210 (2011).
55. W. K. W. Li, Composition of ultraphytoplankton in the central North Atlantic. **122**, 1–8 (1995).
56. A. Z. Worden, J. K. Nolan, B. Palenik, Assessing the dynamic and ecology of marine picoplankton : the importance of eukaryotic component. *Limnol. Ocean.* **49**, 168–79. (2004).
57. E. Teira, *et al.*, Variability of chlorophyll and primary production in the Eastern North Atlantic Subtropical Gyre: Potential factors affecting phytoplankton activity. *Deep. Res. Part I Oceanogr. Res. Pap.* **52**, 569–588 (2005).
58. X. A. G. Morán, Annual cycle of picophytoplankton photosynthesis and growth rates in a temperate coastal ecosystem: A major contribution to carbon fluxes. *Aquat. Microb. Ecol.* **49**, 267–279 (2007).
59. Y. M. Rii, *et al.*, Diversity and productivity of photosynthetic picoeukaryotes in biogeochemically distinct regions of the South East Pacific Ocean. *Limnol. Oceanogr.* **61**, 806–824 (2016).
60. V. S. Smetacek, Role of sinking in diatom life-history cycles: ecological, evolutionary and geological significance. *Mar. Biol.* **84**, 239–251 (1985).
61. C. Sancetta, T. Villareal, P. Falkowski, Massive fluxes of rhizosolenid diatoms : A common occurrence ? *Notes*, 1452–1457 (1989).

554 62. A. F. Michaels, M. W. Silver, Primary production, sinking fluxes and the microbial food
555 web. *Deep. Res.* **35**, 473–490 (1988).
556 63. A. M. Waite, K. A. Safi, J. A. Hall, S. D. Nodder, Mass sedimentation of picoplankton
557 embedded in organic aggregates. *Limnol. Oceanogr.* **45**, 87–97 (2000).
558 64. T. L. Richardson, G. A. Jackson, H. W. Ducklow, M. R. Roman, Carbon fluxes through
559 food webs of the eastern equatorial Pacific: An inverse approach. *Deep. Res. Part I*
560 *Oceanogr. Res. Pap.* **51**, 1245–1274 (2004).
561 65. T. L. Richardson, G. A. Jackson, H. W. Ducklow, M. R. Roman, Spatial and seasonal
562 patterns of carbon cycling through planktonic food webs of the Arabian Sea determined by
563 inverse analysis. *Deep. Res. Part II Top. Stud. Oceanogr.* **53**, 555–575 (2006).
564 66. S. L. C. Giering, *et al.*, High export via small particles before the onset of the North Atlantic
565 spring bloom. *J. Geophys. Res. Ocean.* **121**, 2268–2285 (2016).
566 67. G. Dall'Olmo, K. A. Mork, Carbon export by small particles in the Norwegian Sea.
567 *Geophys. Res. Lett.*, 1–6 (2014).
568 68. T. L. Richardson, G. A. Jackson, Small Phytoplankton and Carbon Export from the
569 Surface Ocean. *Science (80-.).*, 838–840 (2007).
570 69. K. G. J. Nierop, G. J. Reichart, H. Veld, J. S. Sinninghe Damsté, The influence of oxygen
571 exposure time on the composition of macromolecular organic matter as revealed by
572 surface sediments on the Murray Ridge (Arabian Sea). *Geochim. Cosmochim. Acta* **206**,
573 40–56 (2017).
574 70. E. Kristensen, M. Holmer, Decomposition of plant materials in marine sediment exposed
575 to different electron acceptors (O2, NO3−, and SO42−), with emphasis on substrate origin,
576 degradation kinetics, and the role of bioturbation. *Geochim. Cosmochim. Acta* **65**, 419–
577 433 (2001).
578 71. B. Dauwe, J. J. Middelburg, P. M. J. Herman, Effect of oxygen on the degradability of
579 organic matter in subtidal and intertidal sediments of the North Sea area. *Mar. Ecol. Prog.*
580 *Ser.* **215**, 13–22 (2001).
581 72. D. E. Canfield, Factors influencing organic carbon preservation in marine sediments.
582 *Chem. Geol.* **114**, 315–329 (1994).
583 73. H. E. Hartnett, R. G. Keil, J. I. Hedges, A. H. Devol, Influence of oxygen exposure time on
584 organic carbon preservation in continental margin sediments. *Nature* **391**, 572–574
585 (1998).
586 74. K. A. Koho, *et al.*, Microbial bioavailability regulates organic matter preservation in marine
587 sediments. *Biogeosciences* **10**, 1131–1141 (2013).
588 75. M. M. M. Kuypers, R. D. Pancost, I. A. Nijenhuis, J. S. Sinninghe Damsté, Enhanced
589 productivity led to increased organic carbon burial in the euxinic North Atlantic basin
590 during the late Cenomanian oceanic anoxic event. *Paleoceanography* **17**, 3-1-3–13
591 (2002).
592 76. M. Rodrigo-Gámiz, S. W. Rampen, S. Schouten, J. S. Sinninghe Damsté, The impact of
593 oxic degradation on long chain alkyl diol distributions in Arabian Sea surface sediments.
594 *Org. Geochem.* **100**, 1–9 (2016).
595 77. A. W. Jacobel, *et al.*, Deep Pacific storage of respired carbon during the last ice age:
596 Perspectives from bottom water oxygen reconstructions. *Quat. Sci. Rev.* **230** (2020).
597 78. W. Lu, *et al.*, I/Ca in epifaunal benthic foraminifera: A semi-quantitative proxy for bottom
598 water oxygen in a multi-proxy compilation for glacial ocean deoxygenation. *Earth Planet.*
599 *Sci. Lett.* **533**, 116055 (2020).
600 79. A. Rosell-Melé, *et al.*, Precision of the current methods to measure the alkenone proxy
601 U37K′ and absolute alkenone abundance in sediments: Results of an interlaboratory
602 comparison study. *Geochemistry, Geophys. Geosystems* **2** (2001).
603 80. J. P. Dunne, B. Hales, J. R. Toggweiler, Global calcite cycling constrained by sediment
604 preservation controls. *Global Biogeochem. Cycles* **26**, 1–14 (2012).
605 81. O. Cartapanis, D. Bianchi, S. L. Jaccard, E. D. Galbraith, Global pulses of organic carbon
606 burial in deep-sea sediments during glacial maxima. *Nat. Commun.* **7**, 10796 (2016).
607 82. IOCCG, "Remote Sensing of Ocean Colour in Coastal , and Other Optically-Complex ,

Waters" (2000).
83. S. B. Groom, *et al.*, Satellite ocean colour: Current status and future perspective. *Front. Mar. Sci.* **6** (2019).
84. C. W. Brown, J. A. Yoder, Cocolithophorid blooms in the global ocean. *J. Geophys. Res.* **99**, 7467–7482 (1994).
85. D. Blondeau-Patissier, J. F. R. Gower, A. G. Dekker, S. R. Phinn, V. E. Brando, A review of ocean color remote sensing methods and statistical techniques for the detection, mapping and analysis of phytoplankton blooms in coastal and open oceans. *Prog. Oceanogr.* **123**, 123–144 (2014).
86. H. M. Dierssen, R. C. Smith, Bio-optical properties and remote sensing ocean color algorithms for Antarctic Peninsula waters. **105**, 26301–26312 (2000).
87. S. Sathyendranath, G. Cota, V. Stuart, H. Maass, T. Platt, Remote sensing of phytoplankton pigments: A comparison of empirical and theoretical approaches. *Int. J. Remote Sens.* **22**, 249–273 (2001).
88. H. Claustre, S. Maritonera, The Many Shades of Ocean Blue. *Ocean Sci.* **302**, 1514–1515 (2003).
89. G. Volpe, *et al.*, The colour of the Mediterranean Sea: Global versus regional bio-optical algorithms evaluation and implication for satellite chlorophyll estimates. *Remote Sens. Environ.* **107**, 625–638 (2007).
90. H. Claustre, *et al.*, Is desert dust making oligotrophic waters greener? *Geophys. Res. Lett.* **29**, 107-1-107–4 (2002).
91. D. Stramski, J. Tegowski, Effects of intermittent entrainment of air bubbles by breaking wind waves on ocean reflectance and underwater light field. *J. Geophys. Res.* **106**, 31345–31360 (2001).
92. J. J. Cullen, The deep chlorophyll maximum: Comparing vertical profiles of chlorophyll a. *Can. J. Fish. Aquat. Sci.* **39**, 791–803 (1982).
93. J. Huisman, N. N. Pham Thi, D. M. Karl, B. Sommeijer, Reduced mixing generates oscillations and chaos in the oceanic deep chlorophyll maximum. *Nature* **439**, 322–325 (2006).
94. J. E. O'Reilly, *et al.*, SeaWiFS Postlaunch Calibration and Validation Analyses, part 3. *NASA Tech. Memo.* **11**, 1–49 (2000).

Figures and Tables

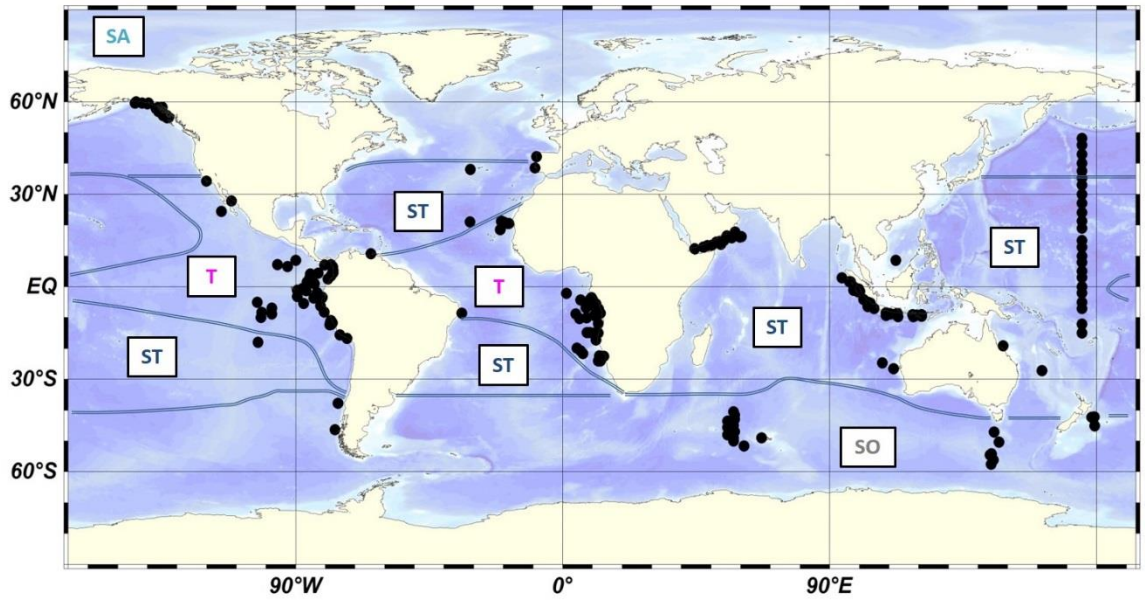

Fig. 1. Global core-top sediments distribution. Lines delineate distinct biogeochemical regions defined on the basis of temperature and nutrient concentration (44) *Abbreviations: subarctic (SA), subtropics (ST), tropics (T) and Southern Ocean (SO).*

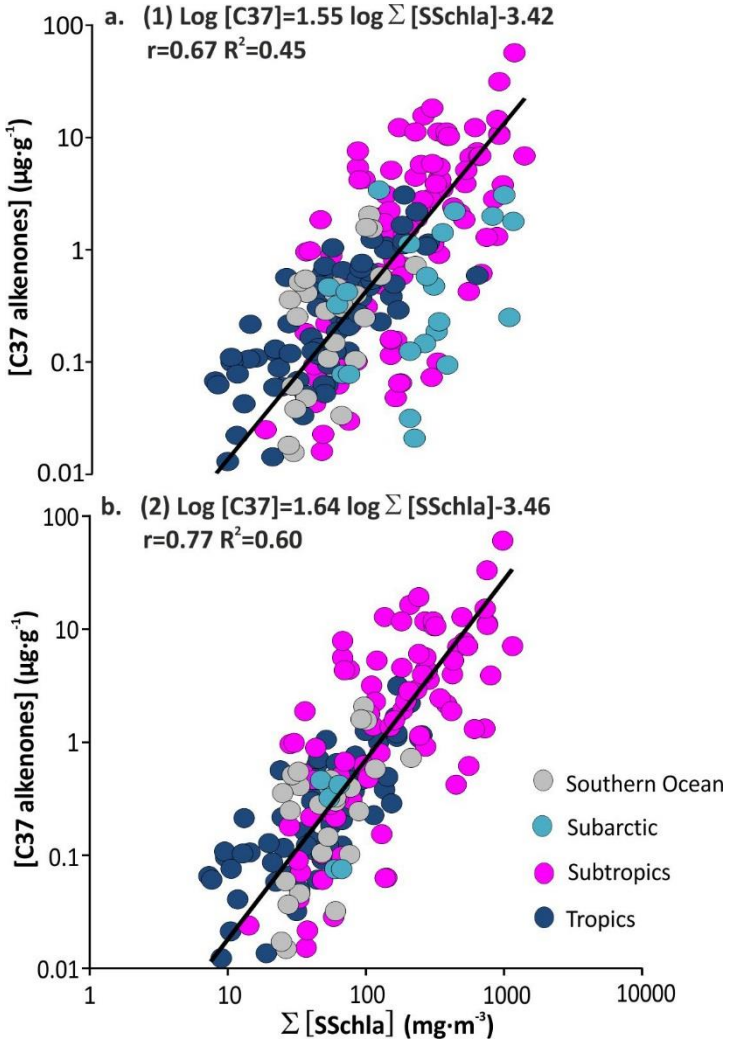

Fig. 2. Global correlations between sedimentary C_{37} alkenones concentration and the sum of sea-surface chlorophyll-*a* (SSchla) concentration from 1997 to 2017. **a.** includes the whole compilation, and **b.** includes regions presenting RMS log errors lower than 31% between remote sensing and *in situ* SSchla. Samples are classified by biogeochemical regions as defined in Fig. 1.

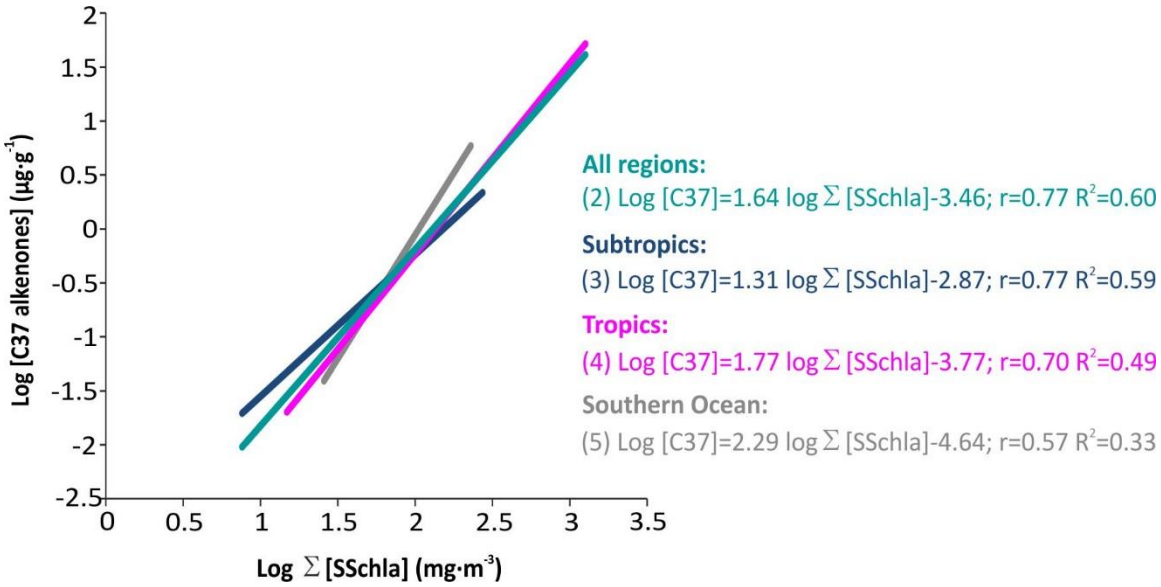

Fig. 3. Regional correlations between sedimentary C_{37} alkenones concentration and the sum of sea-surface chlorophyll-*a* (SSchla) concentration from 1997 to 2017. Different colours for lines and text indicate the evaluated biogeochemical regions, which are defined in Fig. 1.

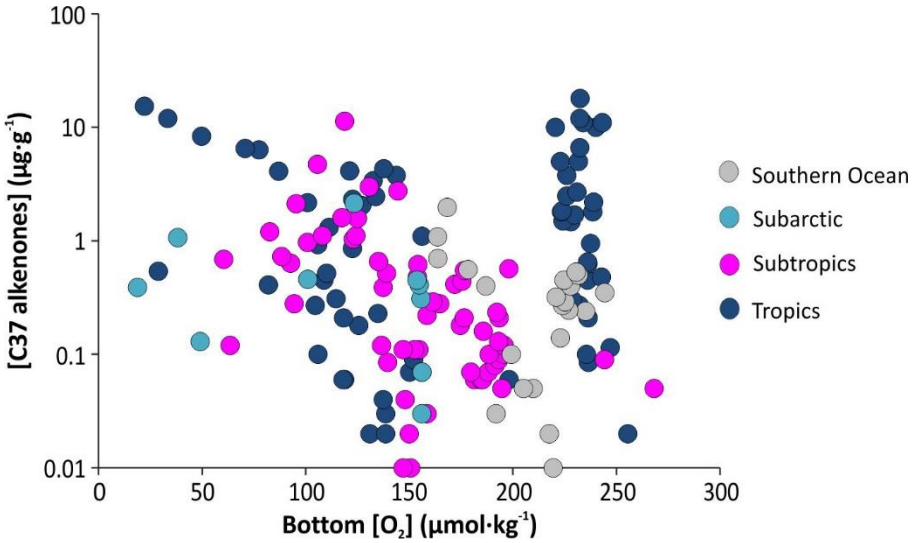

Fig. 4. Global comparison of sedimentary C_{37} alkenones concentration and oxygen concentration in bottom waters. Different colours for lines and text indicate the evaluated biogeochemical regions, which are defined in Fig. 1.

674

675 **Table 1.** Equation coefficients and errors from correlations in Fig. 2 and 3. Log[C_{37}
676 alkenones]=a·log∑[SSchla]+b. *Abbreviations: sea-surface chlorophyll-a (SSchla),* coefficient of
677 correlation (r), *coefficient of determination (R^2), root-mean square logarithmic error (RMS log error),*
678 *number of samples (n).*
679

Equation	Region	a	b	r	R^2	RMS log error (%)	n
1	Global	1.55	-3.42	0.67	0.45	53	226
2	Global	1.64	-3.46	0.77	0.60	38	194
3	Subtropics	1.31	-2.87	0.77	0.59	31	75
4	Tropics	1.77	-3.77	0.70	0.49	46	88
5	Southern Ocean	2.29	-4.64	0.57	0.33	35	26

680
681
682
683